AD-A079 471 AIR FORCE AVIONICS LAB WRIGHT-PATTERSON AFB OH F/G 17/7
PASSIVE FIBER OPTIC GYRO STUDY.(U)
OCT 79 T L WILLIAMSON , D A WILLE
UNCLASSIFIED AFAL-TR-79-1197

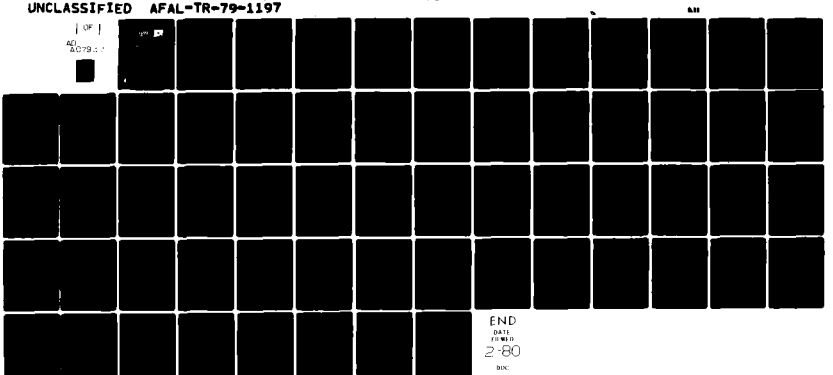

END
DATE FILMED
2-80
DDC

AFAL-TR-79-1197

LEVEL II

PASSIVE FIBER OPTIC GYRO STUDY

DR. T. L. WILLIAMSON
DR. D. A. WILLE
ELECTRO-OPTICS TECHNOLOGY BRANCH
ELECTRONIC TECHNOLOGY DIVISION

OCTOBER 1979

TECHNICAL REPORT AFAL-TR-79-1197
Final Report for period 1 May 1979 — 31 July 1979

Approved for public release; distribution unlimited.

AIR FORCE AVIONICS LABORATORY
AIR FORCE WRIGHT AERONAUTICAL LABORATORIES
AIR FORCE SYSTEMS COMMAND
WRIGHT-PATTERSON AIR FORCE BASE, OHIO 45433

NOTICE

When Government drawings, specifications, or other data are used for any purpose other than in connection with a definitely related Government procurement operation, the United States Government thereby incurs no responsibility nor any obligation whatsoever; and the fact that the government may have formulated, furnished, or in any way supplied the said drawings, specifications, or other data, is not to be regarded by implication or otherwise as in any manner licensing the holder or any other person or corporation, or conveying any rights or permission to manufacture, use, or sell any patented invention that may in any way be related thereto.

This report has been reviewed by the Information Office (OI) and is releasable to the National Technical Information Service (NTIS). At NTIS, it will be available to the general public, including foreign nations.

This technical report has been reviewed and is approved for publication.

TOM L. WILLIAMSON
Electro-Optics Techniques and
Applications Group
Electro-Optics Technology Branch

KENNETH R. HUTCHINSON, Chief
Electro-Optics Techniques and
Applications Group
Electro-Optics Technology Branch

FOR THE COMMANDER

RONALD F. PAULSON, Chief
Electro-Optics Technology Branch
Electronic Technology Division

"If your address has changed, if you wish to be removed from our mailing list, or if the addressee is no longer employed by your organization please notify RADC (OCSC) Griffiss AFB, NY 13441 to help us maintain a current mailing list".

Copies of this report should not be returned unless return is required by security considerations, contractual obligations, or notice on a specific document.

AFSC-Griffiss AFB, NY 1988—80

SECURITY CLASSIFICATION OF THIS PAGE *(When Data Entered)*

REPORT DOCUMENTATION PAGE

READ INSTRUCTIONS BEFORE COMPLETING FORM

1. ~~REPORT NUMBER~~ AFAL-TR-79-1197	2. GOVT ACCESSION NO.
3. RECIPIENT'S CATALOG NUMBER	
4. TITLE *(and Subtitle)* PASSIVE FIBER OPTIC GYRO STUDY	5. ~~TYPE OF REPORT & PERIOD COVERED~~ FINAL REPORT, 1 May 1979 – 31 July 1979
6. PERFORMING ORG. REPORT NUMBER	
7. AUTHOR(s) T. L. Williamson, D. A. Wille	8. CONTRACT OR GRANT NUMBER(s)
9. PERFORMING ORGANIZATION NAME AND ADDRESS AIR FORCE AVIONICS LABORATORY, AFAL/DHO-2, WPAFB, OH 45433	10. PROGRAM ELEMENT, PROJECT, TASK AREA & WORK UNIT NUMBERS 99912000
11. CONTROLLING OFFICE NAME AND ADDRESS Same	12. REPORT DATE October 1979
	13. ~~NUMBER OF PAGES~~ 56
14. MONITORING AGENCY NAME & ADDRESS *(if different from Controlling Office)* Same	15. SECURITY CLASS. *(of this report)* Unclassified
	15a. DECLASSIFICATION/DOWNGRADING SCHEDULE

16. DISTRIBUTION STATEMENT *(of this Report)*

Approved for public release; distribution unlimited.

Tom L. Williamson

17. DISTRIBUTION STATEMENT *(of the abstract entered in Block 20, if different from Report)*

Douglas A. Wille

18. SUPPLEMENTARY NOTES

19. KEY WORDS *(Continue on reverse side if necessary and identify by block number)*

Gyro
Fiber Optic
Sagnac

20. ABSTRACT *(Continue on reverse side if necessary and identify by block number)*

The report summarizes the principles of operation of the passive fiber optic gyro. It starts with a discussion of the Sagnac effect and proceeds to a theoretical prediction of the optimum shot noise limited performance. An overview of the major requirements and problems associated with the principal components follows. This leads to a discussion of the signal processing, some conclusions, and recommendations with respect to specific areas for further investigations.

DD FORM 1 JAN 73 1473 EDITION OF 1 NOV 65 IS OBSOLETE

SECURITY CLASSIFICATION OF THIS PAGE *(When Data Entered)*

Ø11 67Ø

FORWORD

The report summarizes the principles of operation of the passive fiber optic gyro. It starts with a discussion of the Sagnac effect and proceeds to a theoretical prediction of the optimum shot noise limited performance. An overview of the major requirements and problems associated with the principal components follows. This leads to a discussion of the signal processing, some conclusions, and recommendations with respect to specific areas for further investigations.

The study was performed during the period 1 May 1979 through 31 July 1979 by Drs. Tom L. Williamson and Douglas A. Wille. It was initiated at the request of Dr. Ronald F. Paulson.

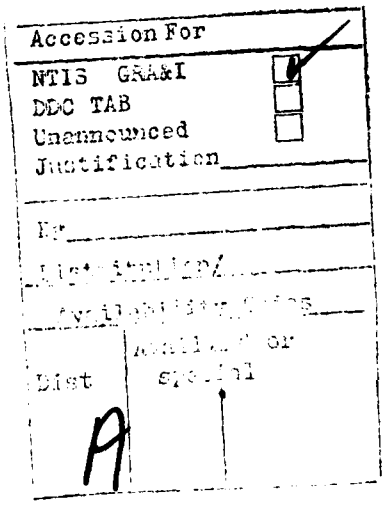

TABLE OF CONTENTS

LIST OF ILLUSTRATIONS

SECTION I

INTRODUCTION

1.0 INTRODUCTION

It is the intent of this report to give an overview of the passive fiber optic gyro, its principles of operation, and its potential performance, as well as a discussion of some of the problems and unknowns associated with its implementation.

The report starts with the principles of operation of the gyro leading to a theoretical prediction of the optimum shot noise limited performance. An overview of the major requirements and problems associated with the principal components follows. This leads to a discussion of the signal processing, some conclusions, and recommendations with respect to specific areas for further investigations.

SECTION II

PRINCIPLE OF OPERATION

2.0 SAGNAC EFFECT

The first demonstration of the feasibility of an optical experiment capable of indicating rotation was constructed by Sagnac in 1913. A description of Sagnac's experiment together with related work by other experimenters is given by Post [1].

The basis of the Sagnac effect is that if an interferometer is constructed in which counter rotating beams describe a complete circuit before interfering, it is found that the resultant interference fringes can be affected by rotating the plane of the interferometer. The effect can be described relativistically but is complicated by the fact that the effect is due to an acceleration, and, therefore special relativity must be used with care. Sagnac's interferometer was constructed as shown in Figure 1.

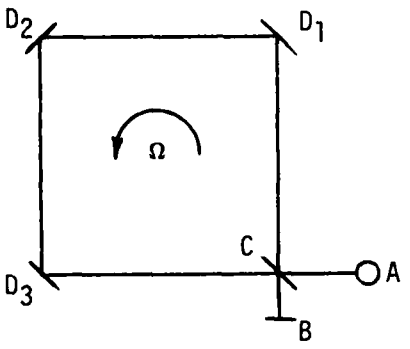

Figure 1. Schematic of Sagnac's interferometer. A = light source; B = observer; C = beam splitter; D_1,D_2 & D_3 are corner mirrors.

When the whole interferometer with light source and fringe detector is set in rotation with an angular rate of Ω radians/ second, a fringe shift ΔZ with respect to the fringe position of the stationary interferometer is observed. This fringe shift is given by the formula

$$\Delta Z = 4\vec{\Omega}\cdot\vec{A}/\lambda_o c \qquad (1)$$

where A is the area enclosed by the light path. The free space wavelength is λ_o and the free space speed of light is c.

If the case is considered where the optical path is circular with signals injected so that one will propagate in each direction as illustrated in Figure 2. The time required for the clockwise

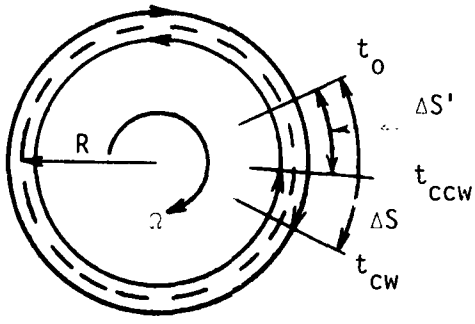

Figure 2. Simplified Interferometer

beam to travel from the point of injection to the point of extraction (same physical point on the ring) is given by

$$t_{cw} = \frac{2\pi R + \Delta S}{c} \qquad (2)$$

where R is the radius of the ring, ΔS is the amount that the ring has rotated, and c is the speed of light.

$$\Delta S = t_{cw}\, \Omega R \qquad (3)$$

Substituting into Equation 2 yields

$$t_{cw} = \frac{2\pi R}{c - \Omega R} \qquad (4)$$

For light travelling in the counterclockwise direction the optical path is shortened and

$$t_{ccw} = \frac{2\pi R - \Delta S'}{c}$$

$$= \frac{2\pi R}{c + \Omega R} \qquad (5)$$

The time difference between the two paths is

$$\Delta t = t_{cw} - t_{ccw}$$

$$= 2\pi R \left(- \frac{1}{c + \Omega R} + \frac{1}{c - \Omega R} \right)$$

$$= 2\pi R \left(\frac{2\Omega R}{c^2 - \Omega^2 R^2} \right) \qquad (6)$$

For rotation rates of interest, $\Omega^2 R^2 \ll c^2$, thus Equation 6 reduces to

$$t = \frac{4\pi R^2 \Omega}{c^2} = \frac{4\,\Omega A}{c^2} \qquad (7)$$

The corresponding change in fringe pattern is given by

$$\Delta Z = \Delta t_v = \Delta tc/\lambda$$

$$= \frac{4\Omega Ac}{c^2\lambda}$$

$$= \frac{4\Omega A}{\lambda c} \qquad (8)$$

which is the expression for the Sagnac effect as given by Equation 1. It has been assumed that the rotation is in the plane of the interferometer so the vector dot product reduces to the scalar product. The phase relationship can be determined by

$$\Delta\phi = 2\pi\Delta Z = \frac{8\pi\Omega A}{\lambda c} \qquad (9)$$

The phase difference will produce a change in the intensity of the fringe pattern and is, thus, the basic observable for sensing rotation. It is noted that no consideration was given to any medium that might be in the propagation path. With a careful and complete description of the problem, it can be shown that the effect is independent of the index of refraction of the propagation medium to first order.

A simple extension of the analysis can account for a multiple turn solenoid of the simple loop. For a solenoid with N turns, starting with Equation 3, it follows that t_{cw} can be replaced by Nt_{cw} resulting in

$$\Delta\phi = \frac{8\pi NA\Omega}{\lambda c} \qquad (10)$$

The resulting fiber ring interferometer will be of the form shown in Figure 3.

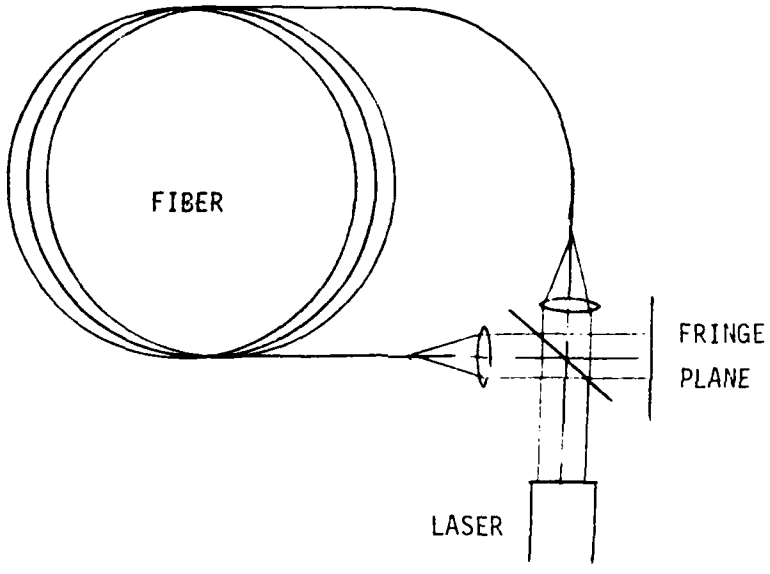

Figure 3. Fiber Ring Interferometer

2.1 INTERFERENCE PATTERN

The amplitude of each of the signals exiting the ring (or solenoid) can be written in the form

$$A \cos(kz - \omega t + \delta + K) \qquad (11)$$

where z is the path length, ω is the radian frequency, t is the time, δ is the phase shift resulting from the Sagnac effect, and K is an additional phase shift. When the two signals are added, the resulting amplitude squared term is given by

$$\begin{aligned} A_T^2 &= (A_1 + A_2)^2 \\ &= (A_1 \cos(kz - \omega t + \delta_1 + K_1) + \\ &\qquad A_2 \cos(kz - \omega t + \delta_2 + K_2))^2 \qquad (12) \\ &= A_1^2 \cos^2(kz - \omega t + \delta_1 + K_1) + \\ &\quad A_2^2 \cos^2(kz - \omega t + \delta_2 + K_2) + \\ &\quad 2A_1A_2 \cos(kz - \omega t + \delta_1 + K_1) \cos(kz - \omega t + \delta_2 + K_2) \end{aligned}$$

Taking the time average of A_T^2 over a period $t = 1/\omega$, gives for the first terms

$$A_1^2 \frac{1}{t} \int_0^t \cos^2(kz - \omega t + \delta_1 + K_1) \, dt =$$

$$A_1^2 \frac{1}{t} \int_0^t [1/2 + \cos 2(kz - \omega t + \delta_1 + K_1)] \, dt = (1/2)A_1^2 \qquad (13)$$

since the time average of the high frequency term is zero over t.

Using the identity

$$\text{Cosx Cos y} = 1/2[\ \text{Cos}(\ x + y) + \text{Cos}\ (\ x - y\ )] \quad (14)$$

the cross product term can be written as

$$A_1A_2[\ \text{Cos}(\ \delta_1 - \delta_2 + K_1 - K_2) + \text{Cos}(2kz - 2\omega t + \delta_1 + \delta_2 + K_1 + K_2)] \quad (15)$$

Averaging over τ gives

$$\frac{A_1A_2}{\tau} \int_0^{\tau} \text{Cos}(\ \delta_1 - \delta_2 + K_1 - K_2)dt =$$

$$A_1A_2\ \text{Cos}(\ \delta_1 - \delta_2 + K_1 - K_2) \quad (16)$$

The second term in Equation 15 integrates to zero. Collecting terms results in

$$\bar{A}_T^{\,2} = 1/2[A_1^{\,2} + A_2^{\,2}] + A_1A_2\text{Cos}(\Delta\phi - \psi\ ) \quad (17)$$

where $\Delta\phi = \delta_1 - \delta_2$ is the Sagnac phase shift and $\psi = K_1 - K_2$ is the nonreciprocal phase shift. If the amplitudes are balanced, ($A_1 = A_2 = A$), then

$$\bar{A}_T^{\,2} = A^2\ [\ 1 + \text{Cos}\ (\ \Delta\phi - \psi\ )\ ] \quad (18)$$

or in terms of power

$$P = P_0\ (\ 1 + \text{Cos}(\ \Delta\phi - \psi\ )) \quad (19)$$

where P_0 is the total power into the interferometer (lossless).

Using Equation 19, the value of the nonreciprocal phase shift that will result in maximum sensitivity can be determined. To maximize the dependency on ψ

$$\frac{\partial P}{\partial \psi} = 0$$

$$= -P_0 \, \mathrm{Sin}(\Delta\phi + \psi) \qquad (20)$$

for small $\Delta\phi$ this requires

$$\mathrm{Sin}\ \psi = 0$$

or

$$\psi = n\pi/2 \qquad (21)$$

Under this condition, choosing $\psi = -\pi/2$

$$P = P_0 [\, 1 + \mathrm{Cos}\, (\Delta\phi - \pi/2)]$$

$$= P_0 [\, 1 + \mathrm{Sin}\, \Delta\phi] \qquad (22)$$

Thus small changes in $\Delta\phi$ occur at the position where the slope of the fringe variation is a maximum.

2.2 SHOT NOISE LIMITATION

The power that is available for sensing the rotation with the $\pi/2$ phase shift is given by Equation 22 as

$$P = P_o[\ 1 + \mathrm{Sin}\ \Delta\phi\ ]$$
$$= P_o[\ 1 + \Delta\phi\ ] \qquad (23)$$

for $\Delta\phi$ small. This can be written as

$$P' = P + \Delta P \qquad (24)$$

where $\Delta P = \Delta\phi P_o$, and $P = P_o$, resulting in the ratio

$$\frac{\Delta P}{P} = \Delta\phi\ . \qquad (25)$$

If the power is detected by a detector with quantum efficiency η , the signal current is given by

$$S = \eta q P/\hbar\omega \qquad (26)$$

where q is the electronic charge. The shot noise inherent in the signal is [2]

$$S_N = \sqrt{2qSB} \qquad (27)$$

where B is the detection bandwidth.

If the shot noise is taken as the minimum detectable change in signal, i.e.

$$\Delta S = S_N, \qquad (28)$$

then

$$\frac{\eta q \Delta P}{\hbar\omega} = [\ 2q(\eta qP/\hbar\omega)B\ ]^{1/2} \qquad (29)$$

or

$$\frac{\Delta P}{P} = \left[2\hbar\omega B/\eta P \right]^{1/2} \qquad (30)$$

Equating this to Equation 25 results in a minimum detectable phase shift of

$$\Delta\phi = \left[2\hbar\omega B/\eta P \right]^{1/2} \qquad (31)$$

This expression applies only to the case where the nonreciprocal phase shift is $\pi/2$. Other values of the phase shift will result in less sensitivity.

2.3 QUANTUM NOISE LIMITATION

With a signal power P, the effective number of photons arriving at the detector is

$$N = P/\hbar\omega \; . \qquad (32)$$

The mean squared fluctuation is

$$\overline{N}^2 = N = P/\hbar\omega \qquad (33)$$

resulting in a noise current

$$i_N = \left[q^2 \eta PB/\hbar\omega \right]^{1/2} \qquad (34)$$

where it is assumed that the noise spectrum is "white" in the bandwidth of interest.

Setting the minimum detectable change in signal equal to the quantum noise results in

$$\frac{\eta q \Delta P}{\hbar\omega} = \left[q^2 \eta PB/\hbar\omega \right]^{1/2}$$

or $$\frac{\Delta P}{P} = [\ \hbar\omega B/\eta P\ ]^{1/2} \qquad (35)$$

For the case with maximum sensitivity, $\psi = \pi/2$,

$$\frac{\Delta P}{P} = \Delta\phi \qquad (36)$$

then

$$\Delta\phi = [\ \hbar\ \omega B/\eta P\ ]^{1/2} \qquad (37)$$

which is $1/\sqrt{2}$ of the corresponding shot noise limitation.

2.4 COMBINED SHOT AND QUANTUM NOISE LIMITATION

Since the two processes are independent, the mean squared fluctuations can be added. The combined limitation is then just the combination of Equations 31 and 37 (combined as signal power) and is given by

$$\Delta\phi = [(3\hbar\omega/\eta P)B]^{1/2}. \qquad (38)$$

2.5 SHOT NOISE LIMITED SENSITIVITY

The overall sensitivity of the gyro can be obtained for the shot noise limited case by combining Equations 10 and 31, i.e.

$$\Delta\phi = \frac{8\pi\ NA\Omega}{\lambda c} = [\ 2\hbar\omega B/\eta P\ ]^{1/2} \qquad (39)$$

or on solving for Ω ,

$$\Omega = \frac{\lambda c}{8\pi NA}\ [\ 2\hbar\omega B/\eta P\ ]^{1/2} \qquad (40)$$

Taking into account the attenuation in the fiber, which can be represented by

$$P = P_0 \, 10^{-\alpha L/10} \tag{41}$$

where P_0 is the initial power, α is the attenuation in db/km, and L is the length of the fiber in kilometers, Equation 40 becomes

$$\Omega = \frac{\lambda c}{8\pi NA} \left[2\hbar\omega B/\eta P_0 \right]^{1/2} 10^{\alpha L/20}$$

$$= \frac{\lambda c}{4\pi RL} \left[2\hbar\omega B/\eta P_0 \right]^{1/2} 10^{\alpha L/20} \tag{42}$$

since $NA = RL/2$.

From the above expression the optimum fiber length can be determined by maximizing the dependency of Ω on the length.

$$\frac{\partial \Omega}{\partial L} = 0$$

$$= \frac{\lambda c}{4\pi R} \left[2\hbar\omega B/\eta P_0\right]^{1/2} \frac{\partial}{\partial L} \left[\frac{10^{\alpha L/20}}{L} \right] \tag{43}$$

or $$-\frac{10^{\alpha L/20}}{L^2} + \frac{\alpha}{20L} \log_e 10 \cdot 10^{\alpha L/20} = 0$$

$$\alpha L = 20/\log_e 10$$

$$\alpha L = 8.68 \tag{44}$$

The optimum length for the fiber can then be determined at any

wavelength provided the attenuation of the fiber is known.

At the optimum fiber length $10^{\alpha L/20} = e$, and

$$\Omega = \frac{\lambda c e}{4\pi RL} \left[2\hbar\omega B/\eta P_o \right]^{1/2}, \qquad (45)$$

which is the shot noise limiting sensitivity for the particular set of parameters.

SECTION III

OPTICAL FIBERS

3.0 INTRODUCTION

The development of fiber optics has been driven by the requirements for long distance communication links and has resulted in single mode optical waveguides with losses that are approximately at the theoretical limit. Relatively poor fibers have losses that are determined by impurity absorption and scattering by surface and volume irregularities. In the past few years, fiber technology has advanced to the point that losses are now determined by the fundamental thermodynamic limits set by the optical interaction with the elementary excitations of the fiber materials.

3.1 LOSS MECHANISMS

The ultimate loss mechanisms are optical interactions with density fluctuations (Rayleigh scattering), photon-phonon interactions with longitudinal acoustic phonons (Brillouin scattering), and photon-phonon interactions with optical phonons (Raman scattering). The cross section for Raman scattering is an order of magnitude smaller than that for Brillouin scattering and can be neglected. In multicomponent fiber materials fluctuations in composition can also cause scattering, but this does not appear to be important in the doped silica fibers. It has been suggested that material defects can provide local distortions in the binding energy of the glass and, thus, introduce band tailing effects for absorption bands outside the region of transparency, but recent loss measurements suggest that this effect is also negligible.

Cummins[3] has provided a derivation of the thermodynamics of scattering and shows that the ratio of the scattered intensity I to the incident intensity I_o is given as

$$\frac{I}{I_o} = \frac{\pi^2}{r^2\lambda_o^4} v^2 \langle(\Delta\varepsilon)^2\rangle \qquad (46)$$

where r is the distance from the scatterer, v is the scattering volume, and ε is the dielectric constant. With further manipulation, it is then shown that the total scattering is given by

$$\frac{I}{I_o} = \frac{\pi^2}{r^2\lambda_o^4} kT\beta_T v \left(\rho\frac{\partial\varepsilon}{\partial\rho}\right)_T^2 \qquad (47)$$

where β_T is the isothermal compressibility and ρ is the density. As an alternate treatment, we can regard ε as a function of entropy and pressure and write

$$\langle(\Delta\varepsilon)^2\rangle = \left(\frac{\partial\varepsilon}{\partial S}\right)_P^2 \langle(\Delta S)^2\rangle + \left(\frac{\partial\varepsilon}{\partial P}\right)_S^2 \langle(\Delta P)^2\rangle \qquad (48)$$

The ΔS term leads to a non-propagating entropy fluctuation which is the Rayleigh scattering component and the ΔP term leads to scattering from sound waves which is the Brillouin component. The further derivation shows

$$\frac{I}{I_o} = \frac{\pi^2 v}{r^2\lambda_o^4}\left[\left(\frac{\partial\varepsilon}{\partial T}\right)_P^2 \frac{kT^2}{\rho C_p} + \left(\rho\frac{\partial\varepsilon}{\partial\rho}\right)_S^2 kT\beta_S\right] \qquad (49)$$

The first term is the Rayleigh component, I_C, and the second term is the sum of the Brillouin components, $2I_B$. The ratio of the two is the Landau-Placzek ratio which is given by

$$\frac{I_C}{2I_B} = \frac{C_P - C_V}{C_V} = \gamma - 1 \qquad (50)$$

where $\gamma = C_P/C_V$.
Thus, the Rayleigh component and the sum of the Brillouin components are of similar magnitude. C_P and C_V are the specific heats at constant pressure and constant volume. A typical scattering result is shown in Figure 4, which is taken from Rich's paper[4] and is measured at 90^o to the propagation direction. It shows the central unshifted Rayleigh component and the pair of frequency shifted Brillouin components. Both the Stokes component (phonon creation) and the anti-Stokes component (phonon annihilation) of the Brillouin doublet have frequency shifts determined by the Bragg condition for diffraction from an acoustic wave. Thus,

$$\vec{k}_S = \vec{k}_I \pm \vec{K} \qquad (51)$$

where $\vec{k}_S$ is the wave vector of the scattered optical wave, $\vec{k}_I$ is the incident wave vector, and $\vec{K}$ is the acoustic wave vector. Conservation of energy also gives the condition

$$\omega_S = \omega_I \pm \omega_K \qquad (52)$$

where ω_K is the acoustic frequency.

In Rich's graph small components due to the fiber cladding are also visible. While the cladding Brillouin component does not cause a problem it points out that the cladding must be considered. The worst effect of the cladding is that some of the scattered light propagates in the cladding and it is difficult to separate it from the guided light of the core region at the output end of

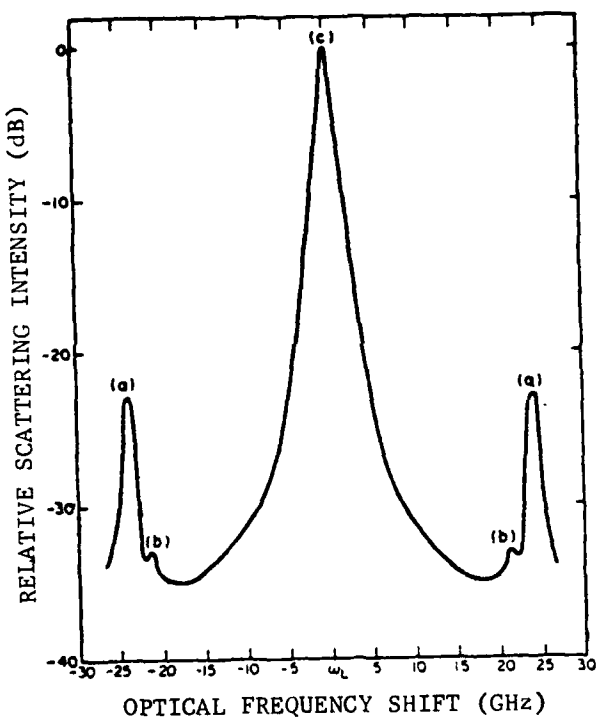

Figure 4. Scattering Spectrum of a Silica Core Borosilicate Clad Fiber. (from T.Rich and D.Pinnow, Applied Optics, 13, 1376(1974)

the fiber. This problem can be avoided by using a mode stripper on the fiber. Mode stripping (cladding modes) is accomplished either by immersing the fiber in index matching fluids or by coating the fiber with an optical absorber.

Pinnow[5] calculated the intrinsic scattering loss for fused silica using the expression for the scattering loss, α,

$$\alpha = \frac{8\pi^3}{3\lambda^4} (n^8 p^2) kT\beta_T \qquad (53)$$

where p is the photoelastic coefficient. No derivation was given for this equation but it appears that it should be derivable from Equation 47. Pinnow reasoned that the fluctuations should be frozen in at the solidification temperature of the material rather than room temperature. Thus, for fused silica the temperature is 1700°K. Figure 5 is a graph taken from Pinnow's paper and the numbers agree with the loss measurements given by Niizeki[6].

The results of Miyashita[7] are the best that have been reported to date and the loss curve is included in Figure 6. The fibers have a GeO_2 doped core with a 9.4μ diameter and an overall diameter of 125μ. The large absorption peaks at 1.25μ and 1.4μ are due to OH bands and the increase in absorption beyond 1.6μ is due to intrinsic material absorption. The loss at 1.55μ is 0.2 db/km and is approximately the theoretical limit for loss. In earlier work Niizeki reported a loss of 0.5 db/km at 1.3μ. The 1.3μ region is of interest for communications since the material dispersion is a minimum at that wavelength and is, thus, the

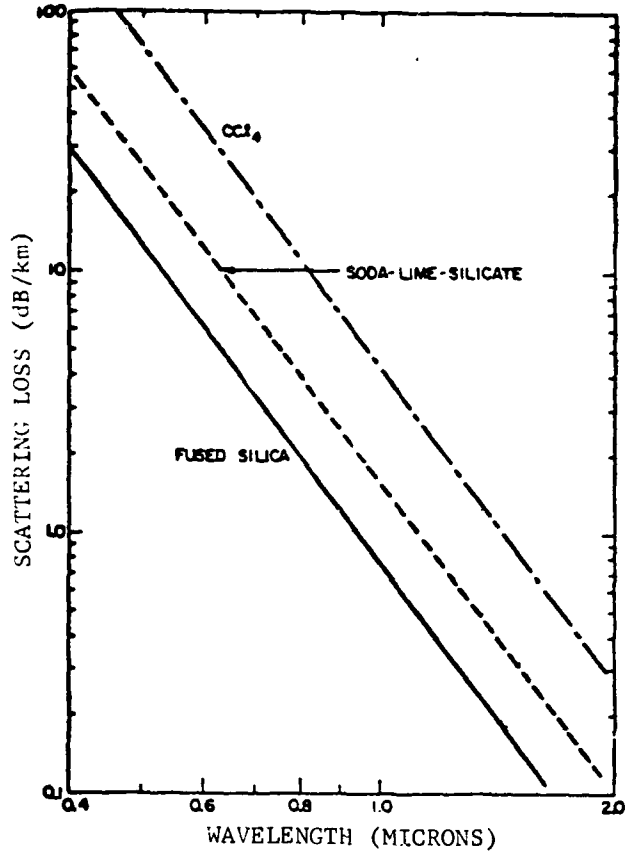

Figure 5. Intrinsic Scattering Loss vs Optical Wavelength for CCl_4, Vitreous Fused Silica, and Soda-Lime-Silicate. (From D. Pinnow, et al, Appl. Phys. Lett. 22, 527(1973).)

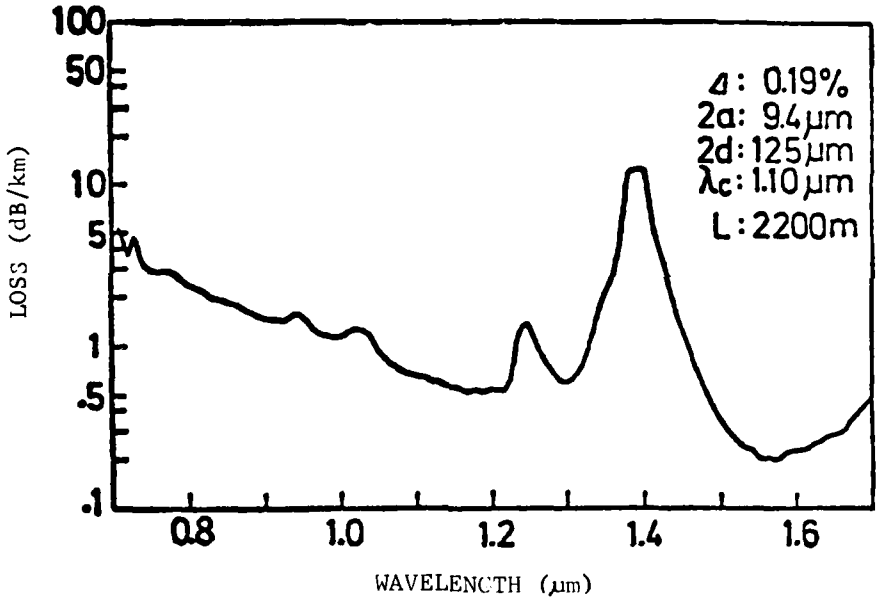

Figure 6. Loss vs Wavelength (from Miyashita, Reference 7)

wavelength of minimum pulse spreading.

A problem area with fibers that is especially important for the gyro application is the birefringence of fibers. A perfect single mode fiber has two orthogonally polarized modes which are degenerate and the fiber will, thus, maintain a given state of polarization. In real fibers it is found that the degeneracy is lifted and mixing between the states can occur. Kapron[8] has considered the polarization states of real fibers and finds a birefringence which is associated with the ellipticity of the fiber core and transverse stress. It was found that both the degree of polarization and the angle of the "fast" axis varied nonlinearly and that the two effects are partially independent. Based on tests with a 200 meter length of fiber, it was found that the degree of polarization was maintained to about 99 percent per kilometer.

Stolen[9] has investigated techniques for introducing birefringence in a fiber to remove the degeneracy of the two orthogonal polarizations. Thus, with sufficient birefringence, coupling between the two polarization states will be reduced. Flats were ground on opposite sides of the preform tube and the drawn fiber had a circular core, a surrounding elliptical cladding region, and a circular substrate region surrounding both. Birefringence is produced by strain between the cladding and substrate regions, producing an index difference of $\delta n \simeq 10^{-5}$. Experiments were performed at 5145 Å and while the best fibers maintained their polarization in the presence of bends and twists, the loss increased from 20 db/km for normal fiber to 35 db/km. Ramaswamy[10] has also successfully investigated techniques for producing birefringence in fibers using more radical grinding of the preform, but no loss measurements were made.

3.2 SCATTERING DISTRIBUTION

Consider a fiber with input power P_i at one end as illustrated in Figure 7a.

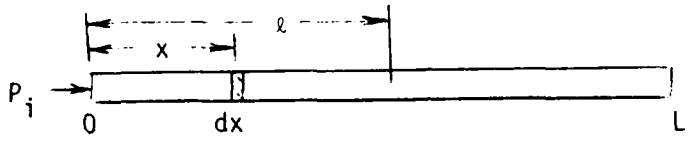

a.

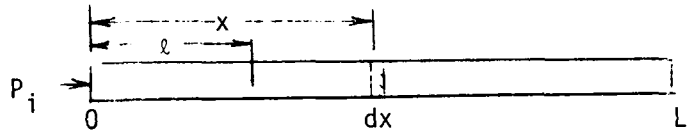

b.

Figure 7. Scattering Geometry

The power at a distance x from the input end is given by

$$P(x) = P_i 10^{-\alpha x/10} \tag{54}$$

where α is the total attenuation coefficient. The scattering from the incremental area dx is then

$$dP(x) = P_i 10^{-\alpha x/10} \alpha_s' dx$$

$$(\alpha_s' = (\alpha_s \log_e 10)/10 = 0.23\ \alpha_s) \tag{55}$$

where α_s is the scattering coefficient. Letting the fraction of the scattered light that is trapped in the fiber be F, the total contribution from the element dx can be expressed as

$$dP(x) = FP_i 10^{-\alpha x/10} \alpha_s' dx \tag{56}$$

At any point ℓ greater than x the contribution will be

$$dP(\ell,x) = (FP_i 10^{-\alpha x/10} \alpha_s' dx) 10^{-\alpha(\ell-x)/10} \tag{57}$$

$$= FP_i 10^{-\alpha \ell/10} \alpha_s' dx$$

Integrating over the fiber length up to ℓ gives

$$P(\ell) = FP_i 10^{-\alpha \ell/10} \alpha_s' \ell \tag{58}$$

or at the end of the fiber $\ell = L$ and

$$P(L) = FP_i 10^{-\alpha L/10} \alpha_s' L \tag{59}$$

Equation 59 then represents the total contribution from forward scattering over the length of the fiber.

The backscattered light can be treated in a similar fashion. Referring to Figure 7b, the backscattering from the element dx can be written as

$$dP(x) = BP_i 10^{-\alpha x/10} \alpha_s' dx \tag{60}$$

where B is the fractional amount of backscattered light that is trapped in the fiber. At any point $\ell < x$

$$dP(\ell) = BP_i 10^{-\alpha x/10} \alpha_s' dx 10^{-\alpha(x-\ell)/10}$$

$$= BP_i 10^{-2\alpha x/10} 10^{\alpha \ell/10} \alpha_s' dx \qquad (61)$$

The total backscattered power at ℓ is then given by

$$P(\ell) = \int_{\ell}^{L} dP(x)$$

$$= BP_i \alpha_s' 10^{\alpha \ell/10} \int_{\ell}^{L} 10^{-2\alpha x/10} dx$$

$$= \frac{BP_i \alpha_s'}{a2\alpha} \left[10^{-\alpha \ell/10} - 10^{-\alpha(2L-\ell)/10} \right] \qquad (62)$$

where $a = (\log_e 10)/10 = 0.23$. At the input end of the fiber $\ell = 0$ and the total backscattered power is given by

$$P(0) = \frac{BP_i \alpha_s}{2\alpha} \left[1 - 10^{-2\alpha L/10} \right] \qquad (63)$$

The coefficients F and B have been calculated by Lin[11] for a fused silica cored fiber with borosilicate glass cladding and found to be of the order of 10^{-3} with mode stripping.

A comparison of the forward scattering and backscattering to the unscattered output power for $F=B= 10^{-3}$ is shown in Figure 8. From this it can be seen that at the optimum condition the scattering components are significantly lower than the unscattered component.

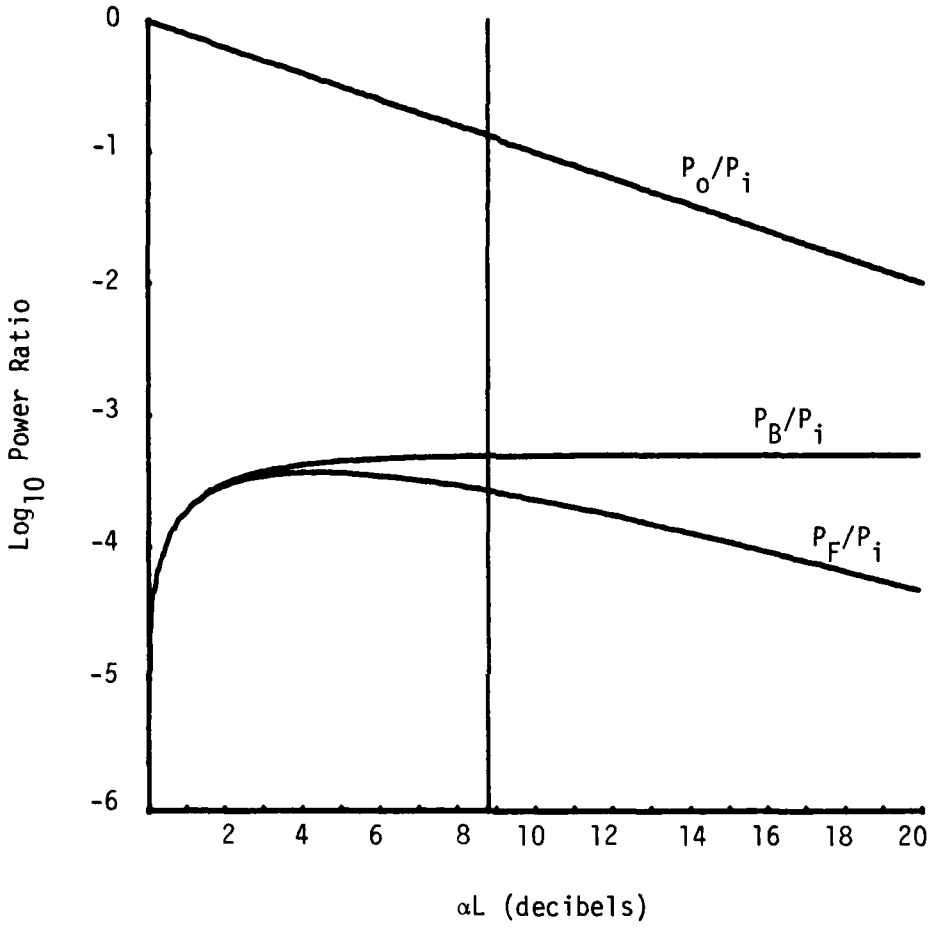

Figure 8. Comparison of Output Power to Forward and Backward Scattered Power Levels as a Function of αL. ($F = B = 10^{-3}$)

SECTION IV

SOURCE CONSIDERATIONS

4.0 INTRODUCTION

The choice of a source for the passive fiber optic gyro is based on requirements ranging from overall size to the thermal stability of the output wavelength. In order for the total gyro package to be small, self-contained and stable, it is desirable that the source be compatible with an integrated optical design. The transmission characteristics of the optical fibers and the overall dependency of the sensitivity of the Sagnac effect on wavelength provide a bias on the selection of wavelength. The requirements for stability and accuracy in the interferometer places restrictions on the linewidth and long term stability of the source. This combination of requirements leads to the selection of a diode laser operating in the .8 to 1.6 micrometer range as the desirable source at the present time. The following sections will expand on some of the considerations that influence the selection of the source.

4.1 WAVELENGTH CONSIDERATIONS

The limiting sensitivity of the gyro as given by Equation 42 is dependent on the choice of wavelength as illustrated by

$$\Omega = \frac{\lambda c}{4\pi RL} \left(\frac{2\hbar\omega B}{\eta P_o} \right)^{1/2} 10^{\alpha L/20}$$

$$= \frac{\sqrt{\lambda} c}{4\pi RL} \left(\frac{2hcB}{\eta P_o} \right)^{1/2} 10^{\alpha L/20} \qquad (64)$$

In addition α is dependent on wavelength as illustrated in Figure 6.

The competing dependencies are that as the wavelength gets longer ($\lambda < 1.6\mu$) the fiber is less lossy, but the interferometer becomes less sensitive with increasing wavelength. The sensitivity at the optimum fiber length as a function of laser power is plotted in Figure 9 using the loss coefficients of Table 1.

λ	α (db/km)
1.55μ	0.2
$1.3\ \mu$	0.5
1.06μ	0.7
0.85μ	2.0

Table 1. Loss Coefficients for Fibers at Selected Wavelengths.

Figure 10 shows the variation of sensitivity with fiber length and input power level at a wavelength of 0.85μ. From this figure it can be seen that an inertial grade gyro ($\Omega < 10^{-3}$ earth rate) is theoretically possible with a fiber length in the 10-100 meters range, depending on power level.

Figure 11 illustrates the dependency of sensitivity on source wavelength for a gyro with a fixed fiber length of 1 kilometer. In general, for fiber lengths significantly shorter than the optimum, the $\sqrt{\lambda}$ factor dominates and it is advantageous to use the shortest wavelength possible. If, however, the ultimate sensitivity is required, it is desirable to use a longer wavelength to take advantage of the lower fiber loss and longer optimum fiber length.

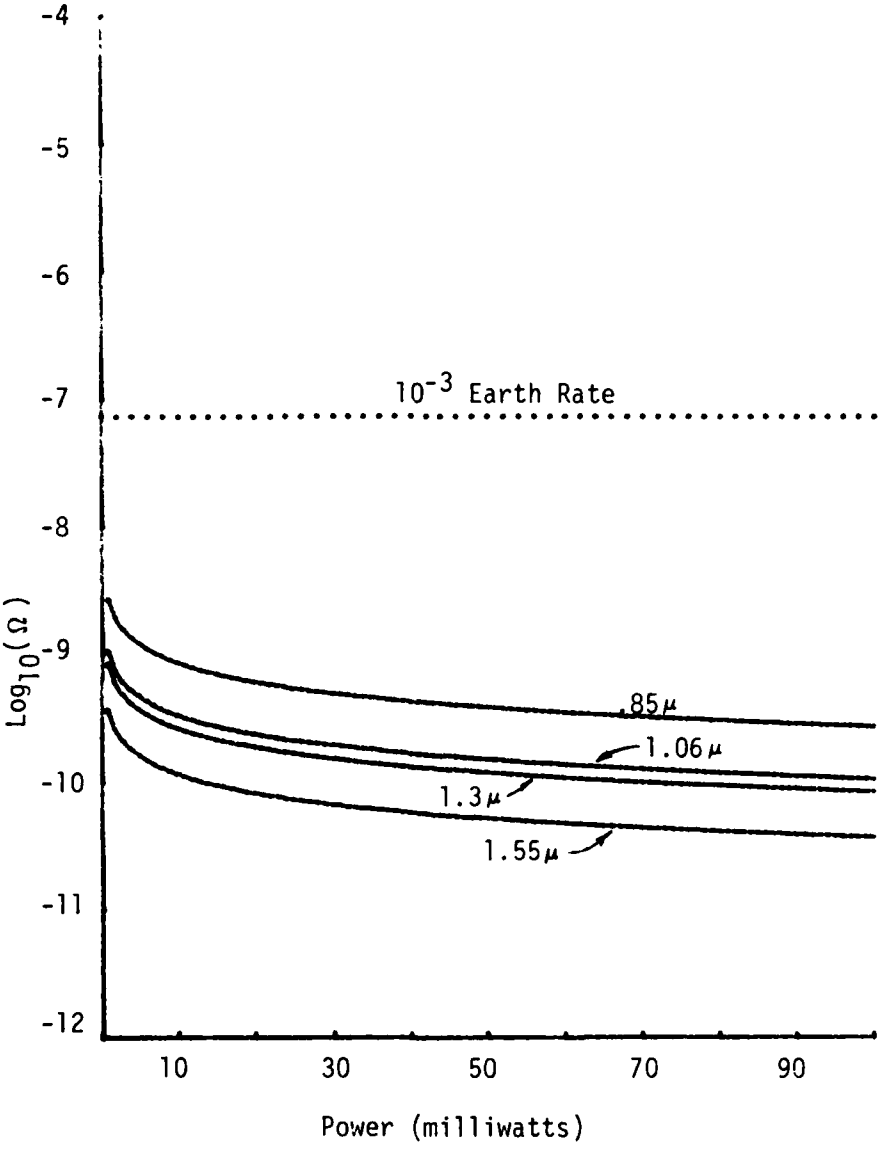

Figure 9. Sensitivity at Optimum Fiber Length
(n=1, B=1, R=10 cm)

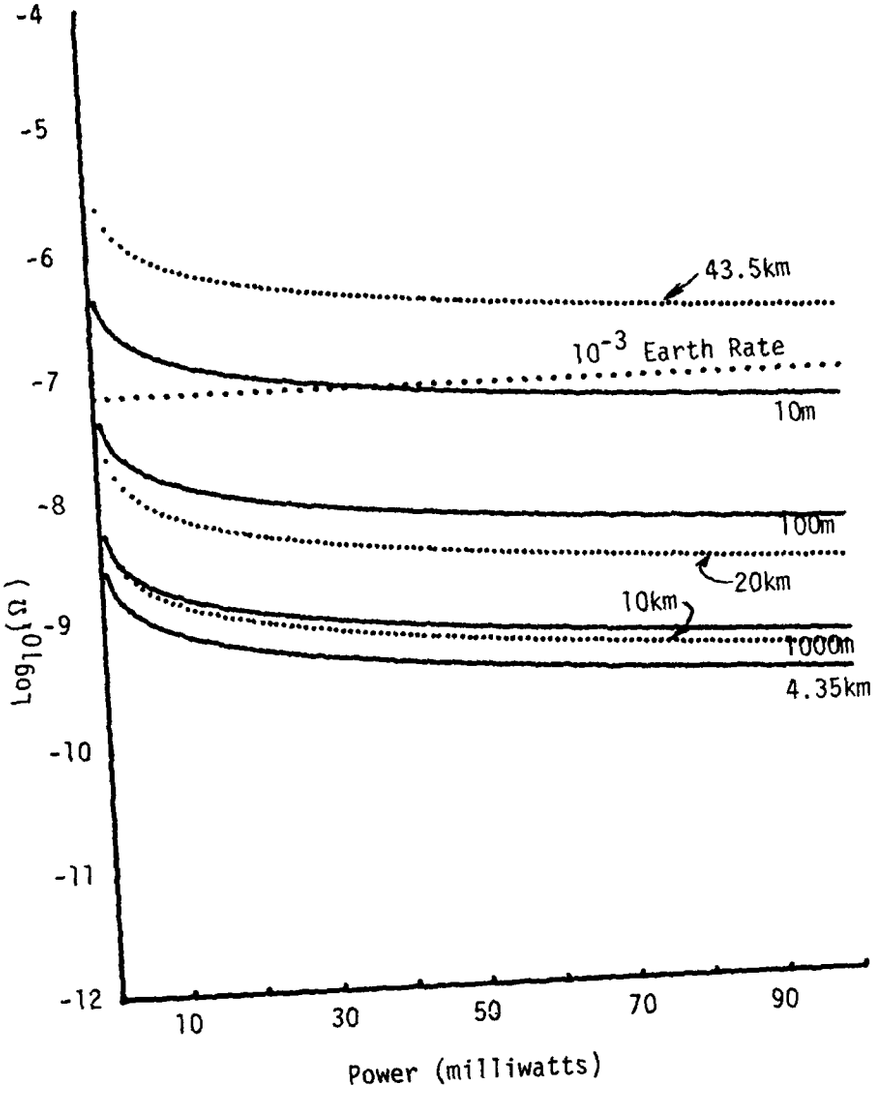

Figure 10. Sensitivity as a Function of Fiber Length ($\lambda = 0.85\mu$)
(Lengths longer than optimum are shown by dotted lines)

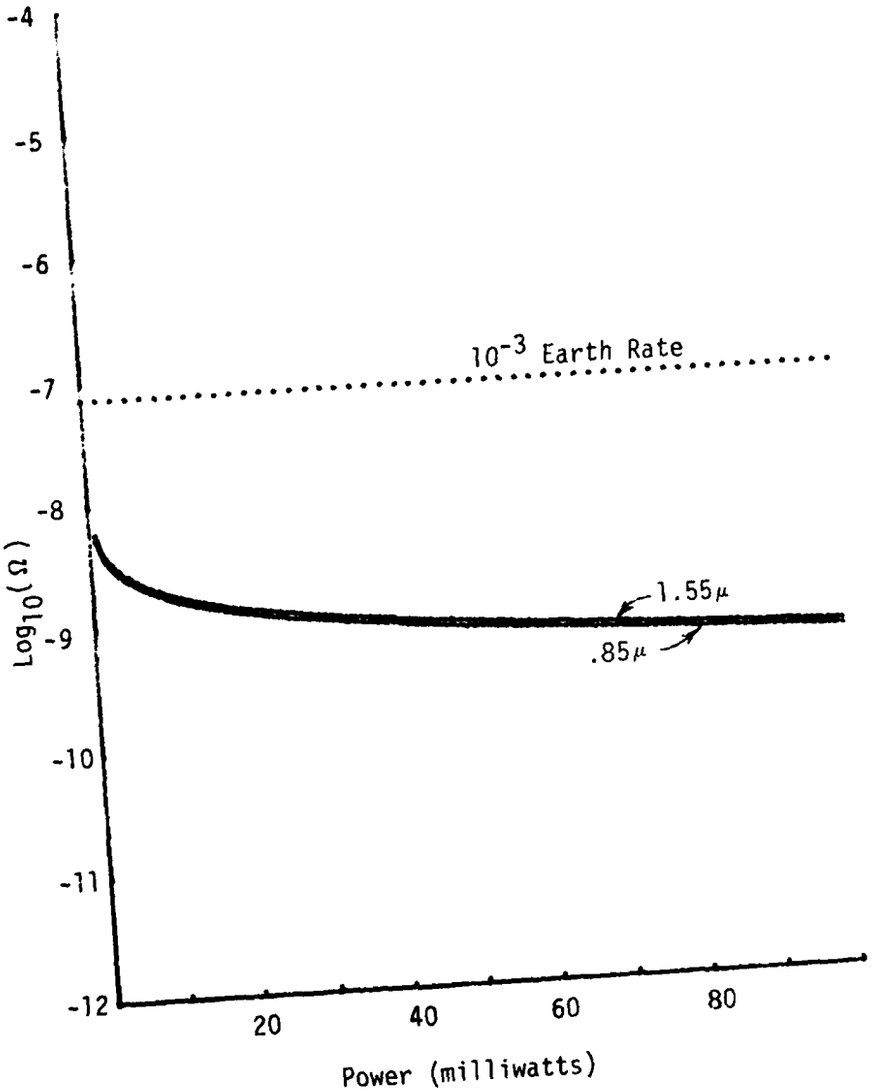

Figure 11. Sensitivity of a 1 Kilometer Fiber Length Gyro at the Wavelengths of 0.85μ and 1.55μ.

4.2 COHERENCE LENGTH

The coherence length of the source places a restriction on the amount of optical path difference that can be tolerated between the two legs of an interferometer without seriously degrading the interference pattern. In the gyro this results in a limitation on optical tolerances, dynamic range, or in the case of a nulling interferometer the dynamic response of the compensating drive.

The coherence length, dl, of a laser can be related to the linewidth, $d\nu$, through the expression

$$dl = c/d\nu \tag{65}$$

or in terms of wavelength by

$$dl = \lambda^2/d\lambda. \tag{66}$$

These relations are illustrated in Figure 12. Point P(1) shows a numerical example, for a 1Å linewidth, and $\lambda = 0.85$, $dl = 7.2 \times 10^{-3}$ meters and $d\nu = 4.15 \times 10^{10}$ hertz.

Aiki[12] has measured a linewidth of 40 megahertz for GaAlAs. As illustrated by point P(2) of Figure 12 this would result in a coherence length of 7.5 meters and linewidth in terms of wavelength of 9.6×10^{-4} Å. In another case Kajimura[13] has directly measured a coherence length of 14 meters for a GaAlAs laser using an interferometer. If these numbers are representative, there should be no problem with coherence length of the laser for the fiber optic gyro providing the laser remains in a single longitudinal and transverse mode.

In Figure 13 the upper graph shows the full set of longitudinal modes under the gain curve, the lower graphs show the mode

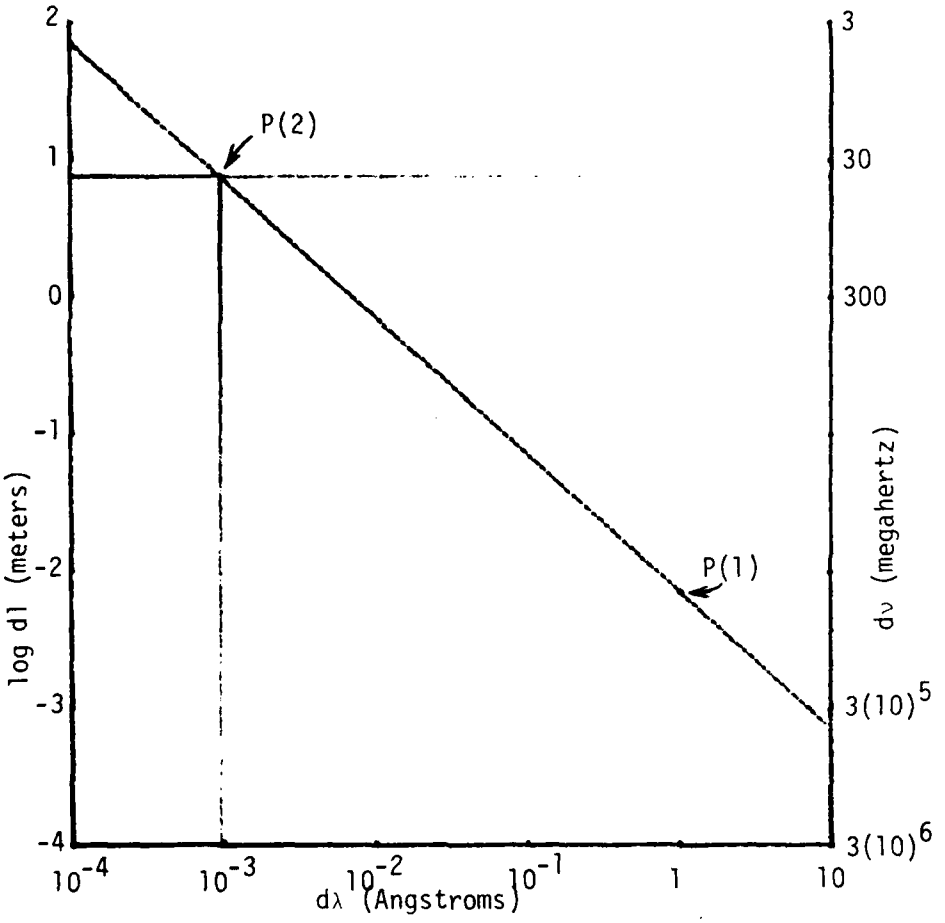

Figure 12. Relationships between Laser Linewidths and Coherence Length.

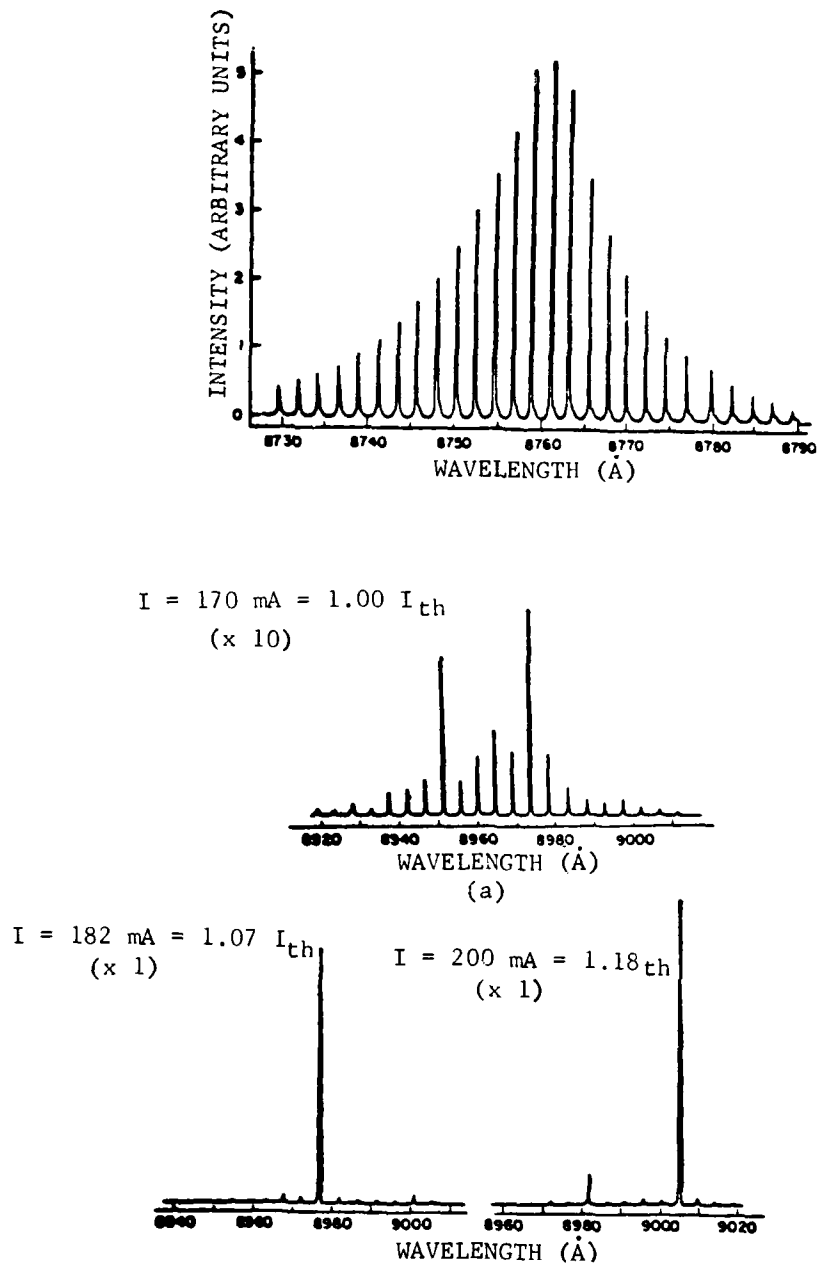

Figure 13. Mode Characteristics for a GaAlAs Laser
(from Paoli,T.,IEEE JQE 11, 276 (1975) Reference 14)

structure for a different laser for various values of current at and above threshold. As can be seen, above threshold the laser is essentially single mode. Thermal effects can cause the gain curve to shift. If the shift is as large as the intermode spacing a transition from one longitudinal mode to another can occur. If two adjacent modes are excited with mode spacings of several angstroms, the effective coherence length will be less than 1mm. In this case very careful adjustment of the two optical paths would be required and could cause a problem.

SECTION V

DETECTORS

5.0 INTRODUCTION

In the preceding section some consideration was given to the desired wavelengths of operation and the main source requirements. It was demonstrated that the ultimate performance of the gyro can be obtained at the longer wavelength region (1.3 - 1.6 micrometer), but the shorter wavelengths are adequate for an inertial grade gyro and, in fact, are more desirable for the shorter fiber lengths. The question to be addressed in this section is the availability of the detectors in the corresponding wavelength regions that meet the requirements of the system. Since the detectors and sources must be considered together, their combined availability will be discussed.

5.1 DETECTOR/SOURCE AVAILABILITY

For the fiber gyro systems considered, power levels are high enough to ensure shot noise limited performance and in no case are modulation rates used which are high enough to cause response time limitations. For instance, semiconductor lasers can be expected to have output powers in the 0.1 mW to 10 mW range. For optimum fiber lengths the transmission of the fiber is 13.5% and if a factor of 10 is allowed for beam splitting and other losses, detector power would be in the 1 - 100 μW range. In the schemes presently under consideration 100 KHz is the highest modulation rate expected. With Si diodes, for instance, 10 nanosecond response times are available and, thus, no difficulty is expected.

The wavelengths of interest for detectors are 0.85 μ, 1.06 μ, 1.3 μ, and 1.55 μ. According to Melchoir[15] Si p-i-n detectors

are available with quantum efficiencies > 90% in the 0.9 μ region and quantum efficiencies of > 70% in the 1.06 μ region. To cover the 1.3 μ and 1.55 μ regions there are Ge avalanche photodiodes with quantum efficiencies of 50% and Ge p-i-n diodes with quantum efficiencies of 60%.

GaAlAs double heterostructure lasers operating at room temperature in the 0.85 μ region are presently available. Single longitudinal mode lasers using some sort of stripe geometry are available in limited quantities and are relatively expensive. It is to be expected that increased availability and reduced cost can occur with further development and increased use.

In the 1.0 - 1.5 μ region the driving force for future development is the communications application. In the 1.3 μ region fiber materials show a minimum dispersion and thus the highest transmission bandwidth. At 1.55 μ there is a minimum in transmission loss and this permits a greater spacing between repeater stations. At least one of these spectral regions and possibly both will receive emphasis that will lead to the development of both sources and detectors. Additional advantages of the longer wavelength region are reduced losses due to splicing and increased resistance to radiation damage.

A potential disadvantage in relying on the communications developments is that detector development is directed toward avalanche photodiodes. Gain is not a requirement for the gyro application and the gain mechanism produces excess noise which is critical to the ultimate accuracy of the gyro. It is not presently clear whether the APD's will operate properly with unity gain. Ando[16] has discussed the Ge APD which is the only APD available for the 1.0 - 1.6 μ region. The Ge APD is not ideal and has high dark current and high multiplication noise. The calculated quantum efficiency of the Ge APD is 90% in the 1.0 - 1.5 μ region.

Tomasetta[17] has discussed development of a GaAlAsSb APD which is expected to be much better than the Ge APD and could have a quantum efficiency of 100% at 1.06 μ and 75% at 1.4 μ with AR coatings.

Yamamoto[18] has discussed fabrication of double heterostructure room temperature lasers in InGaAsP for operation in the 1.1 - 1.67 μ region but it is not known if the lasers were single mode. In earlier work Yamamoto[19] reported lasers in the same material in the 1.25 - 1.35 μ range which were not completely single longitudinal mode. The quoted temperature stability, $d\lambda/dT$, for the lasers was 5 $\mathring{A}/^{o}K$ which is similar to that found with GaAs lasers. Kishino[20] reported an oxide stripe mesa substrate buried heterostructure laser in GaInAsP/InP which operated with a single longitudinal mode and a 0.2 mW output.

It appears that the available sources and detectors should be sufficient for the demonstration of an inertial grade fiber optic gyro, at least at the shorter wavelengths. The ongoing work in the area should provide advancements at a rate commensurate with those of the fibers themselves.

SECTION VI

SIGNAL PROCESSING

6.0 INTRODUCTION

In the preceding sections it has been pointed out that the major components of the passive fiber optic gyro have performance capabilities compatible with the requirements of an inertial grade gyro. A number of questions need to be answered before the ultimate performance can be determined. One of the areas that has not been addressed is that of extracting the rotation rate information from the optical system. In this section only the basic concepts will be addressed. Any more detail would require a specific implementation of the gyro.

6.1 BASIC TECHNIQUES

Following the analysis in Section II, it is apparent that the Sagnac effect can be viewed in terms of either a time delay or as a phase shift. These concepts, although mathematically equivalent, form a natural breakdown for consideration of processing techniques.

Time Delay: If the time difference between the clockwise and counter-clockwise beams is to be used as the measurement of the rotation, Equations 4, 5, and 7 form the basis. Equation 7 extended to include a multiple turn solenoid gives

$$t = \frac{4AN}{c^2}\Omega = \frac{2RL}{c^2}\Omega \qquad (67)$$

$$= 2.2 \times 10^{-15}\Omega$$

for $R = 10$ cm and $L = 10^3$ m. For an inertial grade gyro ($\Omega = 7 \times 10^{-8}$) this would result in a time delay of 1.6×10^{-22} seconds. Times intervals of this magnitude are not presently measurable with integrated circuit type components.

Phase Shift : The phase shift as given by Equation 10 can be measured through the interference and subsequent detection as discussed in Section 2.1. The phase shift resulting from the minimum rotation of an inertial grade gyro is given by

$$\Delta\phi = \frac{4\pi RL}{\lambda c}\,\Omega$$

$$= 4.93\,\Omega \qquad (68)$$

$$= 3.4 \times 10^{-7}$$

The required phase measurement is of the order of 10^{-7} of the fringe width. This accuracy is not beyond that reported in the literature (Reference 21).

Frequency Shift : Since the phase of the interference pattern is directly dependent on the frequency of the interfering beams, the Sagnac phase shift (Equations 10 & 68) can be compensated for by means of a change in frequency of one of the beams. In a fiber of length L and index n the frequency change is given by

$$\frac{2\pi Ln}{c}\,\Delta f = \frac{4\pi RL}{\lambda c}\,\Omega$$

$$\Delta f = \frac{2R}{n\lambda}\,\Omega \qquad (69)$$

$$= 1.57 \times 10^{5}\,\Omega$$

for R = 10 cm, L= 10^3 m, and λ = 0.85 μ. For an inertial grade gyro this corresponds to a minimum frequency shift of 1.1 x 10^{-2} Hz. The frequency corresponding to the fiber length being one period is of the order of 10^5 Hz. The required frequency stability of such a frequency generator would have to be at least 1 part in 10^7. If an acousto-optic modulator is used for the frequency shifting,

the modulation frequency would have to be of the order of 10^8 Hz and the frequency stability would be 1 part in 10^{10} .

6.2 SUMMARY

These examples indicate that the Sagnac effect induced phase shift would be more desirable as the measurement parameter than the time delay. Even the measurement of the phase shift places severe requirements on the stability of the frequency generator and associated electronics. At the present time these restrictions appear to be the limiting factor in the demonstration of the inertial grade passive fiber optic gyro.

SECTION VII

CONCLUSIONS

7.0 CONCLUSIONS

The discussions in the preceding sections have hit on some of the potentials as well as some of the obvious problems of the passive fiber optic gyro. The discussions are in no way complete. Due to the limited time that was available for this study, it was decided that an overview of the total problem would be more beneficial than an in-depth look at a specific area. In some cases enough information is not available to make an accurate assessment. The stimulated Brillouin scattering in the fiber is an example of such an area. The available information is included in Appendix C even though the results are not conclusive.

The passive fiber optic gyro does not suffer from the same problems that plague ring laser gyros, such as lock-in. In principle, the passive fiber optic gyro is capable of measuring rotation rates far better than that required for an inertial grade gyro. For modest laser powers, the passive gyro should have sensitivities in the 10^{-8} radians per second range. These accuracies do not require the use of exotic, beyond the state-of-the-art, lasers, fibers, and detectors. The present limitations are associated with extracting and processing the signal and with the mechanical stability. The signal processing technique should take a maximum advantage of the gyro accuracy while eliminating or balancing out the undesirable variations with time and temperture. This is not a small task.

A number of industrial and government organizations are pursuing fiber gyro developments and in some cases rotation sensitivity measurements have been made. Those measurements that have been reported in the literature are tabulated below. Earth rate is

JPL	2×10^{-4} radians/second	(22)
McDonnell-Douglas	8.7×10^{-3} radians/second	(23)
Rockwell	1.8×10^{-3} radians/second	(24)
NOSC	8.7×10^{-4} radians/second	(25)
MIT (index)	3×10^{-2} radians/second	(26)
(frequency)	6.2×10^{-4} radians/second	(26)
MIT (PARR)	9.7×10^{-5} radians/second	(27)

TABLE 2. Demonstrated Performance

7.2×10^{-5} radians/second and in no case has this sensitivity been demonstrated. Thus, while there is a great potential for fiber gyros, a significant amount of development will be required before practical application can be achieved.

Although the major requirements placed on the components have been discussed and researched for some time, it is felt that several areas warrant further investigation before an accurate assessment of the ultimate performance can be made. Among these areas are:

a. Laser Diodes
   (1) Linewidth
   (2) Mode Jumping
   (3) Noise and Temperature Stability
   (4) Availability in the 1.3 - 1.6 μ region

b. Optical Fibers
   (1) Nonreciprocal Effects
   (2) Polarization Preservation
   (3) Scattering (including stimulated)

c. Detectors
   (1) Availability in the 1.3 - 1.6 μ region
   (2) Low Gain Avalanche Photodiodes

d. Stability and Accuracy of Frequency Sources

e. Stability and Accuracy of A/D Converters

f. General Thermal and Thermal Gradient Effects In Optical Components

g. Potential for Implementation of Signal Processing in Integrated Optics Format

The use of the integrated optics technology will be required for future fiber gyro developments because of the mechanical tolerances required. Shot noise limited performance can require measurement of 10^{-8} fringe and, thus, sub Angstrom mechanical motion in optical components could swamp out the Sagnac phase shift. In the gyro, there are two distinct optical sections. One consists of the laser source, beam splitters, frequency or phase shifters, etc. and the other is the rotation sensitive optical path. In the first case, demonstrated technology is available to fabricate the necessary optical components on a single substrate and, thus, provide the required degree of mechanical stability. In the second case, sufficiently low loss planar waveguides are beyond the present state-of-the-art and fibers will be required. However, mechanical effects are manifested in a different fashion and do not directly produce phase shifts.

In order to arrive at the optimum gyro for a particular mission, consideration must be given not only to the accuracy required but also to the dynamic range. This information is critical to the problem of extracting and using the rotation information, since the

optical system can supply information far in excess of the data handling capability of the digital processing system. For example, the 10^8 accuracy range that is a potential for the gyro would require at least 27 bit accuracy for the digital processing. Therefore, the range of measurements will have to be adjusted to be compatible with military digital data handling systems.

APPENDIX A

SHOT NOISE LIMITATION FOR OTHER PHASE SHIFTS

In addition to the value chosen in Section 2.1, other values of the nonreciprocal phase shift could have been chosen. Consideration is given here to the effect on shot noise limited performance of choosing $\psi = 0$ and $\psi = \pi$.

For the case where $\psi = 0$, from Equation 19

$$P = P_o(1 + \text{Cos } \Delta\phi) \tag{70}$$

When $\Delta\phi$ is small, Cos $\Delta\phi \simeq 1 - \Delta\phi^2/2$. Then

$$P = P_o(2 - \frac{\Delta\phi^2}{2}) \tag{71}$$

Following the procedure in Section 2.2, this results in

$$\frac{\Delta P}{P} = \frac{\Delta\phi^2}{4} \tag{72}$$

Combining with Equation 30,

$$\frac{\Delta\phi^2}{4} = [2\hbar\omega B/\eta P]^{1/2}$$

or

$$\Delta\phi = [32\hbar\omega B/\eta P]^{1/4} \tag{73}$$

For typical values of power and bandwidth, this can result in several orders of magnitude greater limitation than for the case where $\psi = -\pi/2$.

When $\psi = -\pi$, then

$$P = P_o [1 + \text{Cos } (\Delta\phi + \pi)]$$
$$= P_o [1 - \text{Cos } \Delta\phi] \qquad (74)$$

for small $\Delta\phi$

$$P \sim P_o \left(\frac{\Delta\phi^2}{2} \right) \qquad (75)$$

then

$$\Delta S = \frac{\eta q P_o \Delta\phi^2}{2\bar{h}\omega} = [2q^2 (P_o \frac{\Delta\phi^2}{2}) \eta B/\bar{h}\omega]^{1/2} \qquad (76)$$

and

$$\Delta\phi = \frac{2\bar{h}\omega}{\eta q P_o} [q^2 P_o \eta B/\bar{h}\omega]^{1/2}$$

$$\Delta\phi = [\frac{4\bar{h}\omega B}{\eta P_o}]^{1/2} \qquad (77)$$

which is just $\sqrt{2}$ times the limitation for the optimum phase shift. However, for low signal the power on the detector approaches zero and the shot noise will not be the limiting noise source.

APPENDIX B

EVALUATION OF THE EFFECTS OF FINITE LASER LINEWIDTH

We assume the optical wave is of the form $A\cos(\omega t - kz)$ and assume the frequency amplitude distribution is $g(\nu)$. Then the input wave amplitude is

$$A_{input} = A \int \cos \frac{2\pi\nu}{c} (ct - z)\, g(\nu)\, d\nu \tag{78}$$

The two counter propagating waves in the fiber gyro are

$$A_{cw} = A \int \cos \left[\frac{2\pi\nu}{c} (ct - z) + \delta_{cw} \right] g(\nu)\, d\nu$$

$$A_{ccw} = A \int \cos \left[\frac{2\pi\nu}{c} (ct - z) + \delta_{ccw} \right] g(\nu)\, d\nu \tag{79}$$

At the detector the sum amplitude is

$$A_{det} = A \int \left\{ \cos\left[\frac{2\pi\nu}{c} (ct - z) + \delta_{tw} \right] + \cos\left[\frac{2\pi\nu}{c} (ct - z) + \delta_{ccw} \right] \right\} g(\nu)\, d\nu \tag{80}$$

The detected intensity is

$$\begin{aligned} I_{det} &= A^2 \int [\cos(\nu, cw) + \cos(\nu, ccw)]\, g(\nu)\, d\nu \\ &\quad \times \int [\cos(\nu', cw) + \cos(\nu', ccw)]\, g(\nu')\, d\nu' \\ &= A^2 \int [\cos(\nu, cw) \cos(\nu', cw) + \cos(\nu, ccw) \cos(\nu', ccw) \\ &\quad + \cos(\nu, ccw) \cos(\nu', cw) + \cos(\nu, cw) \cos(\nu', ccw)]\, g(\nu)\, g(\nu') \\ &\quad d\nu\, d\nu' \end{aligned} \tag{81}$$

where the abbreviated notation cos(ν, cw) refers to the frequency ν and the cw wave etc.

Expanding the first term we have,

$$\cos(\nu, \text{cw})\cos(\nu', \text{cw}) = \cos\left[\frac{2\pi\nu}{c}(ct - z) + \delta_{cw}\right]$$

$$\times \cos\left[\frac{2\pi\nu'}{c}(ct - z) + \delta'_{cw}\right]$$

$$= 1/2\cos[2\pi t(\nu + \nu') - \frac{2\pi Z}{c}(\nu + \nu') + \delta_{cw} + \delta'_{cw}]$$

$$+ 1/2\cos[2\pi t(\nu - \nu') - \frac{2\pi Z}{c}(\nu - \nu') + \delta_{cw} - \delta'_{cw}] \tag{82}$$

where δ'_{cw} is the cw part of the Sagnac shift at frequency ν'.

If we take the time average over a period $t \gg 1/\nu$, the first term is zero and the second term will also be zero unless $\nu = \nu'$. Thus, the first integral in I_{det}/A^2 is

$$\int 1/2\,\delta(\nu - \nu')\,g(\nu)\,g(\nu')\,d\nu\,d\nu' = 1/2\int g^2(\nu)\,d\nu \tag{83}$$

The second integral gives the same result and in the third we can expand as follows,

$$\cos(\nu, \text{ccw})\cos(\nu', \text{cw})$$

$$= 1/2\cos[2\pi t(\nu + \nu') - \frac{2\pi Z}{c}(\nu + \nu') + \delta_{ccw} + \delta'_{cw}]$$

$$+ 1/2\cos[2\pi t(\nu - \nu') - \frac{2\pi Z}{c}(\nu - \nu')]\cos[\delta_{ccw} - \delta'_{cw}]$$

$$- \sin[2\pi t(\nu - \nu') - \frac{2\pi Z}{c}(\nu - \nu')]\sin[\delta_{ccw} - \delta'_{cw}] \tag{84}$$

The first term averages to zero and the second term is zero unless $\nu = \nu'$, thus giving the time average

$$1/2\ \delta(\nu - \nu')\ \cos[\delta_{ccw} - \delta'_{cw}]$$

Thus we have

$$\frac{I_{det}}{A^2} = 1/2 \int g^2(\nu)\, d\nu + 1/2 \int g^2(\nu)\, d\nu$$
$$+ 1/2 \int \delta(\nu - \nu') \cos(\delta_{ccw} - \delta'_{cw})\, g(\nu)\, g(\nu')\, d\nu\, d\nu'$$
$$+ 1/2 \int \delta(\nu - \nu') \cos(\delta'_{ccw} - \delta_{cw})\, g(\nu)\, g(\nu')\, d\nu\, d\nu'$$
$$= \int g^2(\nu)\, d\nu + \int \cos \Delta\psi\ g^2(\nu)\, d\nu \tag{85}$$

If we had allowed an arbitrary fixed phase shift, K, to be included in the cw or ccw wave we would have

$$\frac{I_{det}}{A^2} = \int g^2(\nu)\, d\nu + \int \cos(\Delta\psi + K)\, g^2(\nu)\, d\nu \tag{86}$$

Next consider the second integral. We can write

$$\Delta\psi = \frac{8\pi NA\Omega}{c^2}\ \nu = \alpha\nu \tag{87}$$

and we will assume the $g^2(\nu)$ is symmetric about a center frequency ν_o. Then $g^2 = g^2(\nu - \nu_o)$ and we can define a new variable, $u = \nu - \nu_o$. The second integral then becomes

$$\int \cos(\alpha\nu_o + K + \alpha u)\, g^2(u)\, du$$
$$= \int [\cos(\alpha\nu_o + K) \cos \alpha u - \sin(\alpha\nu_o + K) \sin \alpha u]\, g^2(u)\, du$$
$$= \cos(\alpha\nu_o + K) \int \cos \alpha u\, g^2(u)\, du \tag{88}$$

where the sin αu integral is zero because of the symmetry. We thus have the cos $(\alpha\nu_o + K)$ term multiplied by the Fourier transform of the lineshape function, which identification follows because $g^2(u)$ is symmetric.

We consider two simple cases; first a rectangular function

$g^2(u)$

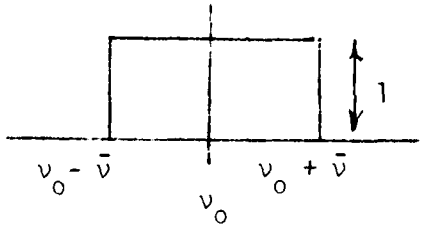

where the transform is

$$g^2(u) \leftrightarrow \frac{2 \sin \alpha\bar{\nu}}{\alpha} \tag{89}$$

and a triangular function

$g^2(u)$

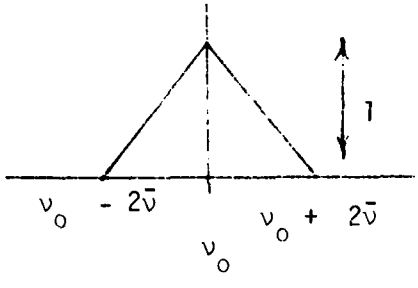

where the transform is

$$g^2(u) \leftrightarrow \frac{2 \sin^2 \alpha\bar{\nu}}{\bar{\nu}\alpha^2} \tag{90}$$

Notice that in both cases the FWHM is $2\bar{\nu}$. Also for both cases

$$\int g^2(\nu)d\nu = 2\bar{\nu} \tag{91}$$

Then for the rectangular function

$$\frac{I_{det}}{A^2} = 2\bar{\nu}\left[1 + \cos(\Delta\psi + K)\frac{\sin \alpha\bar{\nu}}{\alpha\bar{\nu}}\right] \qquad (92)$$

and for the triangular function

$$\frac{I_{det}}{A^2} = 2\bar{\nu}\left[1 + \cos(\Delta\psi + K)\frac{\sin^2 \alpha\bar{\nu}}{\bar{\nu}^2\alpha^2}\right] \qquad (93)$$

For the case of a 4 km fiber, with a coil radius of 10 cm $\alpha = 5.6 \times 10^{-14}\Omega$, and at earth rate $\alpha = 4 \times 10^{-18}$. For GaAs, $\bar{\nu} = 10^7 H_3$ and $\alpha\bar{\nu} = 4 \times 10^{-11}$ which makes the multiplicative factors negligible in both cases.

APPENDIX C

STIMULATED BRILLOUIN SCATTERING

Smith [28] has calculated the critical power level for producing stimulated Brillouin scattering (SBS) in fibers. The expression is

$$P_{crit} = 20\alpha A/\gamma_o \qquad (94)$$

where α is the attenuation coefficient in cm^{-1}, A is the cross sectional area of the fiber and γ_o is the gain coefficient for the process. SBS in the backward direction has the lowest threshold and would be a serious problem since it could deplete the signal beams. The effect of rotation on the backward SBS wave is presently unanalyzed but the SBS would at best produce a background optical noise. Smith calculated P_{crit} = 35 mw for fused silica fiber with a loss of 20 db/km and A = 10^{-7} cm^2. For a fiber with 2 db/km loss the threshold would be only 3.5 mw. A still worse case is the fiber reported by Miyashita[7]. There the loss is 0.2 db/km and the 9μ diameter fiber has an area 0.63 of that in Smith's example. The factor of 160 difference would make the critical power 0.2 mw.

Ippen[29] discussed the SBS problem and showed that

$$P_{crit} = 20A/\gamma_o l_{eff} \qquad (95)$$

where

$$l_{eff} = (1 - e^{-\alpha \ell})/ \alpha \qquad (96)$$

For the case of the optimum length, $e^{-\alpha \ell}$ = 0.135 and

$$P_{crit} = \frac{20\alpha A}{\gamma_o}(1.16) \qquad (97)$$

If, for instance, a fiber length of $\alpha\ell = \alpha\ell_{opt}/3$ is used $e^{-\alpha\ell} = 0.513$ and

$$P_{crit} = \frac{20\alpha A}{\gamma_o}(2.1) \qquad (98)$$

Thus, if SBS becomes a problem at longer wavelengths it may be possible to use a shorter length fiber than optimum to avoid the SBS problem, still retaining some of the advantages of the longer wavelengths. Ippen gives the gain coefficient as

$$\gamma_o = 2\pi n^7 p_{12}^2/c\lambda^2\rho v_s \Delta\nu \qquad (99)$$

While γ decreases with longer wavelength because of the $1/\lambda^2$ term the effect is offset by the decrease in Brillouin linewidth $\Delta\nu$.

REFERENCES

1. E. Post, Rev. Mod. Phys., 39, 475(1967).
2. W. L. Wolfe, Handbook of Military Infrared Technology, Washington, D.C.; U. S. Government Printing Office, 1965 p. 470.
3. H. Cummins and R. Gammon, J. Chem. Phys. 44, 2785(1966).
4. T. Rich and D. Pinnow, Appl. Opt. 13, 1376(1974).
5. D. Pinnow, et al., Appl. Phys. Lett. 22, 527(1973).
6. N. Niizeki, IEEE/OSA Topical Meeting on Integrated and Guided Wave Optics, Salt Lake City, 16 January 1978.
7. T. Miyashita, IEEE/OSA Topical Meeting on Optical Fiber Communications, Washington, D.C., 8 March 1979.
8. F. Kapron, et al., IEEE JQE 8, 222(1972).
9. R. Stolen, et al., Appl. Phys. Lett. 33, 699(1978).
10. V. Ramaswamy, et al., Appl. Phys. Lett. 33, 814(1978).
11. S. Lin and T. Giallorenzi, Appl. Opt. 18, 915(1979).
12. K. Aiki, IEEE JQE 14, 89(1978).
13. T. Kajimura, et al., Appl. Opt. 18, 1812(1979).
14. T. Paoli, IEEE JQE, 11, 276(1975).
15. H. Melchior, et al., Proc. IEEE, 58, 1466(1970).
16. H. Ando, et al., IEEE JQE 14, 804(1978).
17. L. Tomasetta, et al. IEEE JQE 14, 800(1978).
18. T. Yamamoto, Conf. on Laser Engr. and Appl., Washington D. C., May 1979.

19. T. Yamamoto, IEEE JQE 14, 95(1978).

20. K. Kishino, et al., Conf. on Laser Engr. and Appl., Washington, D. C., May 1979.

21. G. E. Moss, et al., Applied Optics 10, No. 11, 2495(1971).

22. W. Goss and R. Goldstein, Opt. Engr. 18, 9(1979).

23. R. Cahill and E. Udd, Opt. Lett. 4, 93(1979).

24. D. Thompson, et al., Appl. Phys. Lett. 33, 940(1978).

25. M. McLandrich and H. Rast, SPIE 157, 127(1978).

26. J. Davis and S. Ezekial, SPIE 157, 131(1978).

27. S. Ezekial and S. Belsamo, Appl. Phys. Lett. 30, 478(1977).

28. R. Smith, Applied Optics, 11, 2489(1972).

29. E. Ippen and R. Stolen, Appl. Phys. Lett. 21, 539(1972).

☆U.S.Government Printing Office: 1979 — 657-084/404